Immunity, Vol. 20, 651, May, 2004, Copyright ©2004 by Cell Press

Erratum

Structural and Functional Analysis of the Costimulatory Receptor Programmed Death-1

In this article (Immunity *20*, 337–347, March 2004), the authors inadvertently omitted the names of two authors; there was also an omission from the Acknowledgments. The corrected sections follow.

Xuewu Zhang, Jean-Claude D. Schwartz, Xiaoling Guo, Sumeena Bhatia, Erhu Cao, Michael Lorenz, Michael Cammer, Lieping Chen, Zhong-Yin Zhang, Michael A. Edidin, Stanley G. Nathenson, and Steven C. Almo

We thank Dr. T. DiLorenzo and M. Roden for insightful discussions, Dr. Z. Dauter for assistance with data collection, and Dr. Brenowitz and S. Morris for assistance with analytical ultracentrifugation experiments. This work was performed at the Analytical Imaging Facility of the Albert Einstein College of Medicine, which is partially supported by the Albert Einstein Cancer Center. This work was supported by grants from the National Institutes of Health (to L.C., M.A.E., S.G.N., and S.C.A.). X.G. and Z.-Y.Z. are supported in part by the G. Harold and Leila Y. Mathers Charitable Foundation.

Immunity, Vol. 20, 337–347, March, 2004, Copyright ©2004 by Cell Press

Structural and Functional Analysis of the Costimulatory Receptor Programmed Death-1

Xuewu Zhang,[1,10] Jean-Claude D. Schwartz,[2,11] Xiaoling Guo,[3,9] Sumeena Bhatia,[2,9] Erhu Cao,[1] Lieping Chen,[7] Zhong-Yin Zhang,[3] Michael A. Edidin,[8] Stanley G. Nathenson,[1,2,*] and Steven C. Almo[4,5,6,*]

[1]Department of Cell Biology
[2]Department of Microbiology and Immunology
[3]Department of Pharmacology
[4]Department of Biochemistry
[5]Department of Physiology and Biophysics
[6]Center for Synchrotron Biosciences
Albert Einstein College of Medicine
Bronx, New York 10461
[7]Department of Immunology
Mayo Clinic
Rochester, Minnesota 55905
[8]Department of Biology
The Johns Hopkins University
Baltimore, Maryland 21218

Summary

PD-1, a member of the CD28/CTLA-4/ICOS costimulatory receptor family, delivers negative signals that have profound effects on T and B cell immunity. The 2.0 Å crystal structure of the extracellular domain of murine PD-1 reveals an Ig V-type topology with overall similarity to the CTLA-4 monomer; however, there are notable differences in regions relevant to function. Our structural and biophysical data show that PD-1 is monomeric both in solution as well as on cell surface, in contrast to CTLA-4 and other family members that are all disulfide-linked homodimers. Furthermore, our structure-based mutagenesis studies identify the ligand binding surface of PD-1, which displays significant differences compared to those present in the other members of the family.

T cell activation and regulation are critically dependent on signals provided by members of the CD28/CTLA-4 costimulatory receptor family. For example, CD28 and ICOS, upon engaging their respective ligands (B7-1/B7-2 and B7RP-1), deliver stimulatory signals that upregulate the activity of the responding T cells (Carreno and Collins, 2002). In contrast, the binding of CTLA-4 to the B7-1/B7-2 ligands negatively regulates T cell activity, resulting in decreased T cell proliferation and decreased cytokine production. Programmed death-1 (PD-1) is another member in this family, sharing ~20% sequence identity with CD28, CTLA-4, and ICOS. Currently, the only two known sequences of PD-1 are the murine and human orthologs that share ~60% identity (Finger et al., 1997). The engagement of PD-1 by its specific ligands, B7-H1 (PD-L1) (Dong et al., 1999) or B7-DC (PD-L2) (Tseng et al., 2001), was reported to inhibit T and B cell proliferation and cytokine production (Freeman et al., 2000; Latchman et al., 2001; Okazaki et al., 2001). The inhibitory signals of PD-1 are mediated, at least in part, by the SHP-2 phosphatase, which is recruited to the phosphorylated Tyr residue in the immuno-tyrosine based switch motif of the cytoplasmic tail of PD-1 and dephosphorylates signal transducers of the TCR or BCR pathways (Latchman et al., 2001; Okazaki et al., 2001). A critical role for PD-1 in immune regulation is highlighted by recent gene disruption studies that demonstrated strain-specific phenotypes: PD-1-deficient C57BL/6(B6) mice develop lupus-like autoimmune proliferative arthritis and glomerulonephritis with IgG3 deposition (Nishimura et al., 1999), while deficiency of PD-1 in BALB/c mice results in a severe autoimmune dilated cardiomyopathy followed by death due to congestive heart failure (Nishimura et al., 2001).

PD-1 and the other receptors in this family are all type I transmembrane glycoproteins composed of an Ig Variable-type (V-type) extracellular domain, a transmembrane domain, and a cytoplasmic tail responsible for the binding of signaling and scaffolding molecules. CD28, CTLA-4, and ICOS are covalently linked homodimers due to the interchain disulfide mediated by the equivalent of Cys122 in CTLA-4 (Schwartz et al., 2002). In contrast, PD-1 cannot form such a covalent dimer as it lacks the analogous Cys residue and it is not known whether it forms noncovalent oligomers. In addition, PD-1 possesses only a single intrachain disulfide in its Ig V-type domain, while CD28, CTLA-4, and ICOS all contain two intrachain disulfides. Another distinct feature of PD-1 is that the CDR3 loop does not contain the conserved XXPPP(F/Y) (X represents any amino acid) motif present in CD28, CTLA-4, and ICOS, which is known to be critical for their ligand binding activities. Consistent with this sequence disparity, PD-1 does not bind B7-1, B7-2, or B7RP-1, and it has not been established whether the CDR3 loop of PD-1 plays a role in binding its own ligands B7-H1 and B7-DC (Latchman et al., 2001; Sharpe and Freeman, 2002). Furthermore, in contrast to other receptors in this family that are only present on T cell surfaces, PD-1 is also expressed on the surface of activated B cells and plays a role in B cell regulation (Agata et al., 1996). Taken together, these distinct features of PD-1 set it apart as a unique member of the costimulatory receptor family. Currently, there are no data bearing on several important issues relevant to the structure and function of PD-1, including the structural similarities and differences between PD-1 and other costimulatory receptors, the ligand binding sites of PD-1, the oligomeric state of PD-1, and the signaling mechanism utilized by the complex of PD-1 and its ligands.

*Correspondence: nathenso@aecom.yu.edu (S.G.N.); almo@aecom.yu.edu (S.C.A.)
[9]These authors contributed equally to this work.
[10]Present address: Xuewu Zhang, Howard Hughes Medical Institute, Department of Molecular and Cell Biology, University of California, Berkley, Berkeley, California 94720.
[11]Present address: Jean-Claude D. Schwartz, Department of Surgery, Emory University Hospital, Atlanta, Georgia 30322.

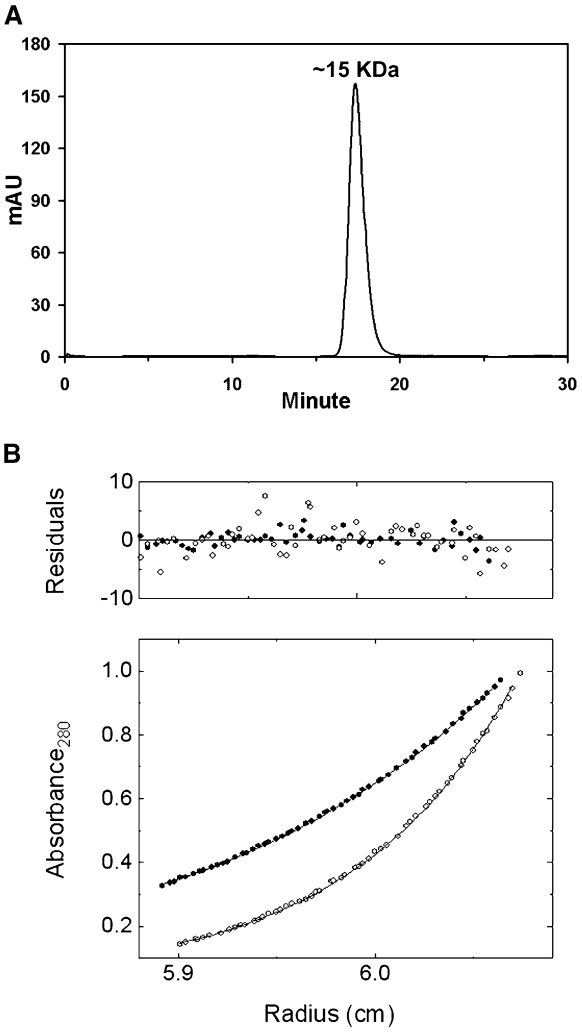

Figure 1. Monomeric State of Murine PD-1

(A) Elution profile of the purified extracellular Ig V-type domain of murine PD-1 from Superdex G75 Gel filtration chromatography. The single monodisperse peak at ~17.5–18 min corresponds to a MW of ~15 kDa.

(B) Determination of the oligomerization state of the Ig V-type domain of murine PD-1 by sedimentation equilibrium. Filled points (closed circles) and open points (open circles) represent data collected at 25,000 rpm and 34,000 rpm, respectively. For clarity, every sixth point is plotted. Lines represent the best fit to a single-component sedimentation model yielding an estimate of the apparent MW, 13.3 kDa. The residuals of the corresponding points are randomly distributed, indicating that there is no oligomerization occurring and that the sample only consists of monomers.

We report here the structural, biophysical, and biochemical features of the Ig V-type domain of murine PD-1. The crystal structure and structure-based mutagenesis studies of PD-1 identified a ligand binding surface that is significantly different from those of the other members of the CD28/CTLA-4 costimulatory receptor family. In addition, our data demonstrate that this soluble form of PD-1 is monomeric both in solution and the crystalline form. More importantly, fluorescence resonance energy transfer (FRET) studies demonstrate that full-length PD-1 is monomeric when expressed on the cell surface. These observations establish differences in oligomeric state between PD-1 and other members of the costimulatory receptor family.

Results

PD-1 Is Monomeric in Solution

The extracellular Ig V-type domain of murine PD-1 was expressed in *E. coli* and refolded in vitro. This purified protein chromatographed as a symmetric monodisperse peak on a calibrated Superdex G-75 (30X1.0) gel filtration column. The elution time of 17.5–18 min corresponds to a molecular weight (MW) of ~15 kDa (Figure 1A), which is very close to the calculated MW of 13296 Da for the recombinant PD-1 monomer. The similarly refolded, purified human PD-1 protein (calculated MW = 14501 Da) also ran as a ~15 kDa monomer on Superdex G-75 gel filtration chromatography (data not shown). The monomeric state of murine PD-1 in solution was confirmed by sedimentation equilibrium analysis (Figure 1B). The data are consistent with a single component model with values within error of the monomeric MW of the recombinant murine PD-1. Various self-association models (i.e., monomer ↔ dimer, monomer ↔ trimer, and monomer ↔ tetramer) were examined and are not consistent with the data. Taken together, these results demonstrated that this soluble form of PD-1 is a stable monomer and does not measurably oligomerize in solution.

PD-1 Is Monomeric when Expressed on the Cell Surface

To examine the oligomeric state of PD-1 in a cellular context, the coding regions for the cyan fluorescent protein (CFP) or yellow fluorescent protein (YFP) were fused to the 3′ end of the full-length murine PD-1 gene. These constructs were cotransfected into CHO cells and the oligomeric state of the full-length protein on the cell surface was evaluated using FRET by photobleaching (Figure 2A). The tandem CFP-YFP fusion protein and full-length disulfide-linked dimeric murine CTLA-4 served as positive controls and gave a broad distribution of FRET efficiencies with averages of 24% ± 8% and 16% ± 5%, respectively (Figure 2B). The data scatter is typical of the CFP/YFP FRET pair (Pentcheva and Edidin, 2001). The FRET efficiency for the tandem CFP-YFP and disulfide-linked CTLA-4 showed no dependence on acceptor intensity (Figure 2C). This behavior is characteristic of a system containing preassociated (i.e., clustered) donor/acceptor molecules, and is fully consistent with the covalent structure of these molecules (Kenworthy and Edidin, 1998). The distribution of FRET efficiencies for the full-length PD-1 constructs is greatly skewed toward lower values (relative to the positive controls) with an average value of 6% ± 4%, slightly but significantly higher than the FRET observed for the negative control (Figure 2B). FRET between CPF-PD-1 and YFP-PD-1 molecules showed a linear dependence on acceptor fluorescence intensity (Figures 2B and 2C). This is characteristic of FRET between randomly distributed molecules and is consistent with the presence of unclustered (i.e., monomeric) PD-1 on the cell surface (Kenworthy and Edidin, 1998). A short form of PD-1 with the cyto-

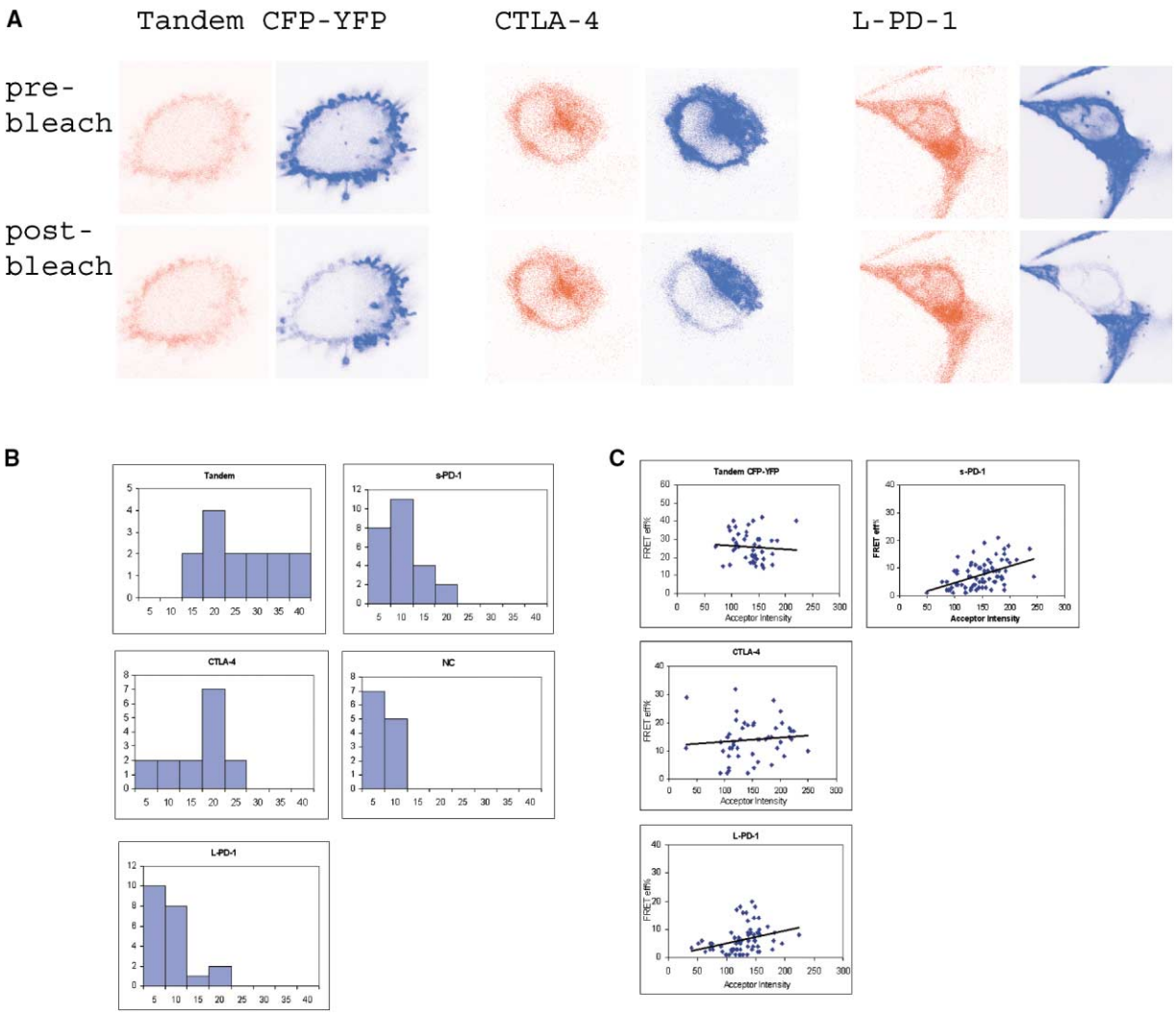

Figure 2. Cellular Behavior of PD-1

(A) Images of CFP and YFP fluorescence on individual cells pre- and postbleaching. For clearer presentation, the color scheme of the images is reversed with CFP and YFP displayed in red and blue, respectively.

(B) Distribution pattern of FRET efficiency (x-axis) as a function of number of cells (y-axis) for various groups as labeled. These data are pooled from four independent experiments, with total 14, 15, 21, and 25 cells examined for the tandem CFP-YFP, CTLA-4, L-PD-1, and S-PD-1, respectively. NC, negative control.

(C) The correlation between the acceptor intensity (expressed as arbitrary units) and the FRET efficiency for individual regions of interest (ROI) is shown for the groups as marked. The total number of ROI analyzed for each group is 60 to 80. The line corresponds to the best linear fit and its slope is the measure of dependence of FRET efficiency on the concentration of acceptor molecules (expressed as acceptor intensity) (Kenworthy and Edidin, 1998).

plasmic tail trimmed to 10 residues displayed spectral properties similar to the long form (Figures 2B and 2C), suggesting that the behavior of the full-length wild-type murine PD-1 is not due to the long (94 amino acids), and likely flexible, cytoplasmic tail. Together the data strongly support the idea that PD-1 is predominantly present as a monomer on the cell surface.

Binding Affinity of the Murine PD-1/B7-H1 Complex

In order to test whether the recombinant PD-1 produced in bacteria retains its biological activity, the interaction between murine PD-1 and the B7-H1-Ig fusion protein was measured by surface plasmon resonance (SPR) using a Biacore X instrument. The results demonstrate that our recombinant murine PD-1 specifically binds B7-H1-Ig coupled to CM5 sensor chips, suggesting that PD-1 refolded from inclusion bodies is biologically active. Equilibrium binding assays were performed to determine the equilibrium dissociation constant (K_d) between murine PD-1 and the B7-H1-Ig fusion protein. Murine PD-1, over a wide range of concentrations (78.0–0.5 μM), was sequentially injected over the sensor chip coupled with murine B7-H1-Ig (Figure 3A). At all concentrations examined, binding reached equilibrium within a few seconds, and similarly, complete dissociation was achieved within a few seconds after termination of the injections. These observations are consistent with fast k_{on} and k_{off} rates for the PD-1/B7-H1 interaction. Nonlin-

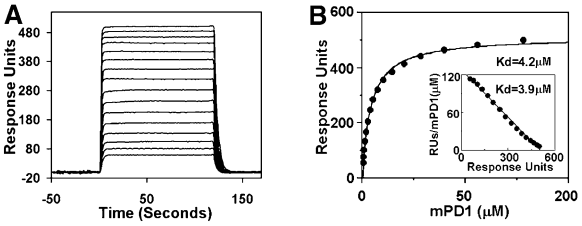

Figure 3. Equilibrium Binding Affinity Measurement for Murine PD-1/B7-H1-Ig

(A) Murine PD-1 over a series of concentrations (started from 78.0 μM and 1.4-fold dilution thereof) was injected over both the experimental flow cell (containing 3621 RUs immobilized murine B7-H1-Ig) and the reference flow cell. The final response at each concentration, represented by the continuous sensorgrams, was obtained by subtracting the response of the control cell from that of the experimental cell.

(B) Nonlinear 1:1 Langmuir fitting and linear Scatchard plot (insert) of the binding data yield K_d of 4.17 ± 0.14 and 3.9 ± 0.07 μM, respectively.

ear 1:1 Langmuir fitting of the binding data yielded a K_d of 4.17 ± 0.14 μM, and linear fitting of the Scatchard plot of the same data resulted in a K_d of 3.90 ± 0.07 μM (Figure 3B). These equilibrium constants observed for PD-1/B7-H1 are comparable to those measured for the CTLA-4/B7 complexes using similar SPR assays (Collins et al., 2002). Crossspecies interaction of human PD-1 with murine B7-H1 has been reported before by several studies (Freeman et al., 2000; Latchman et al., 2001). These observations were confirmed by the same SPR binding assay that demonstrated that recombinant murine and human PD-1s exhibited roughly similar binding affinity for murine B7-H1-Ig (data not shown).

The Structure of Murine PD-1 and a Comparison with that of CTLA-4

The PD-1 monomer displays a two-layer β sandwich topology characteristic of Ig V-type domains, with the front and back sheets formed by the A′GFCC′C″ and ABED strands, respectively (Figure 4A). Cys21 in the B strand and Cys90 in the F strand form an intrachain disulfide, which is a hallmark feature of Ig V-type domains (Metzler et al., 1997). An examination of contacts within the crystal does not identify any candidate dimer interface, consistent with the observed monomeric state of PD-1 in solution and on the cell surface.

Although there is only about 20% sequence identity between their extracellular Ig V-type domains, a superimposition of the structures of murine PD-1 and CTLA-4 monomers demonstrates that they have very similar overall structures as evidenced by the good overlay between most of the equivalent β strands (Figures 5A and 5B) (Ostrov et al., 2000). This structural similarity is confirmed by the low root mean square (rms) deviation of ~1.5 Å between 76 equivalent C_α atoms from PD-1 and CTLA-4. However, there are significant differences between PD-1 and CTLA-4 involving the C″ strand, C′C″ C″D and CDR1 loops. The most pronounced difference is the placement of the C″ strand that participates in the back face in CTLA-4 but participates in the front face in PD-1. Structural differences in the C′C″, C″D and CDR1 loops between PD-1 and CTLA-4 are largely due to their different lengths as shown by the structure-based sequence alignment (Figure 5C). Although the difference in the CDR3 loop between PD-1 and CTLA-4 is less obvious based on the superimposition, detailed structural analyses highlight fundamental differences in this region. In the crystal structures of both murine and human CTLA-4, the CDR3 loops are very rigid as indicated by well-defined electron density and relatively low B factors in this region compared to the rest of the protein (Ostrov et al., 2000; Schwartz et al., 2001; Stamper et al., 2001). This is in part due to the three consecutive Pro residues in the CDR3 loop (^{99}MYPPPY^{104}) that adopt an unusual cis-trans-*cis* conformation that is critical for the ligand binding activity of CTLA-4. In contrast, the CDR3 loop in the present PD-1 structure displays very high B factors and weak electron density compared to the rest of the molecule, indicating this loop in PD-1 is highly flexible.

Notably, nonpolar residues in the front sheet of PD-1 (M31, L32, A47, A48, I93, L95, P97, A99, and I101) form a large hydrophobic patch surrounded by hydrophilic residues, including charged residues D29, K45, K98, and E103 (Figures 4B and 4C), which is reminiscent of the organization present in classical protein-protein interfaces (Bogan and Thorn, 1998). In addition, these nonpolar residues are highly conserved between murine and human PD-1 (Figure 5C). These observations, in combination with the fact that other members in this family (CD28, CTLA-4, and ICOS) all use their front face for ligand binding (Schwartz et al., 2001; Stamper et al., 2001; Wang et al., 2002), suggest that this hydrophobic patch on the front face might be the predominant determinant for ligand binding in PD-1. Another hydrophobic patch on the surface of murine PD-1 formed by residues in the AA′ loop is involved in a crystal contact in the present crystal form. However, residues forming this hydrophobic patch are not conserved between murine and human PD-1 and there is no evidence supporting a role for this region in PD-1 function (Figure 5C).

Ligand Binding Surface of Murine PD-1

Based on the crystal structures of murine PD-1 and the CTLA-4/B7 complexes (Schwartz et al., 2001; Stamper et al., 2001), a series of murine PD-1 mutants (D29A, D29S, M31A, N33A, K45A, N51A, L53A, Q55A, Q55S, V57A, H74S, R81S, I93A, L95A, H96A, P97A, K98A, A99L, I101A, and E103A) were designed for mapping its ligand binding surface. While most of the selected residues were mutated to Ala, several polar residues were mutated to Ser to minimize adverse effects of the mutation on protein refolding and stability. All of the residues selected for mutagenesis have their side chains directed toward solvent, and therefore, their mutations are predicted not to significantly affect the hydrophobic core or structural integrity of the PD-1 protein. The majority of these residues are located in or near the hydrophobic patch on the front face (Figure 1B). All of the mutants except Q55A and I93A were expressed, refolded, and purified at yields comparable to the wild-type. Q55A did not refold under the conditions used to refold the other proteins, which may be the consequence of the in-

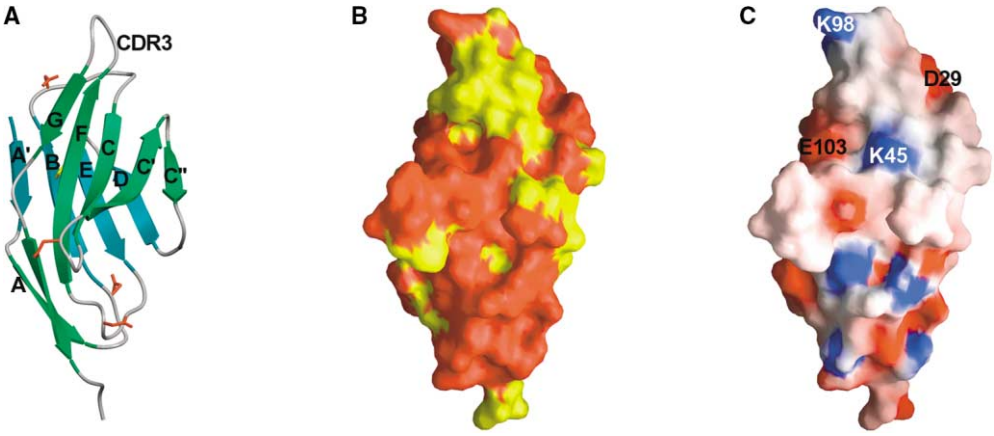

Figure 4. Structure of Murine PD-1

(A) Ribbon diagram of the Ig V-type domain of murine PD-1. The front (green) and back (aqua) sheets are composed of A′GFCC′C″ and ABED strands, respectively. The CDR3 loop is labeled. The intrachain disulfide is shown in yellow. The four potential glycosylation sites are highlighted by showing the side chains of the Asn residues in red.

(B) Hydrophobicity of the molecular surface of murine PD-1. Hydrophobic residues are colored in yellow, whereas hydrophilic residues are colored in red. The orientation of the molecule is similar to that in (A). The large hydrophobic patch on the front face (circled) was hypothesized to be the ligand-binding site.

(C) Electrostatic molecular surface of murine PD-1. Negative and positive potentials are colored in red and blue, respectively. Charged residues surrounding the hydrophobic patch shown in (B) are labeled. The orientation of the molecule is similar to that in (A).

creased hydrophobicity of the protein surface introduced by the mutation, since the Q55S mutant refolded just as well as the wild-type. I93A had a significantly lower refolding yield compared to the wild-type and other mutants, but it was reasonably stable after refolding and adequately well behaved for binding assays. The lower refolding efficiency of I93A might be the consequence of a localized structural perturbation caused by the mutation, as I93 is located at the center of the hydrophobic patch. The purified HA-tagged wild-type and all the refolded mutants eluted as monodisperse peaks from the Superdex G-75 column at ~17 min, slightly earlier than the elution time of the nontagged PD-1 (not shown), consistent with the higher MWs of these epitope tagged proteins. Comparable refolding efficiency and similar behavior on gel filtration chromatography suggest that these mutants refolded correctly and have the same overall structure as the wild-type of murine PD-1. Therefore, the measured differences in binding affinities for the mutants, compared to the wild-type, should directly reflect the contributions of particular residues to the ligand binding activity of murine PD-1.

The binding activities of the HA-tagged and nontagged wild-type PD-1 were compared by injecting these two proteins at the same concentration over the same CM5 sensor chip coupled with murine B7-H1-Ig, which resulted in very similar response levels (data not shown). This result indicates that the HA-tag does not significantly affect the binding activity of PD-1 for its ligand. Therefore, all subsequent binding assays utilized the HA-tagged wild-type and mutants of murine PD-1. The wild-type and mutant proteins, at the same concentration, were sequentially injected over the sensor chips coupled with murine B7-H1-Ig fusion protein, and the response levels of the mutants were compared with that of the wild-type to obtain the relative ligand binding activities of the mutants.

The mutants can be divided into several groups based on their abilities to bind the B7-H1 ligand. K45A, I93A, L95A, I101A, and E103A have unmeasurable or extremely weak binding activity for the ligand compared to the wild-type (Figure 6; see Supplemental Table S2 at http://www.immunity.com/cgi/content/full/20/3/337/DC1), suggesting side chains of these residues are directly involved in and indispensable for the interaction between PD-1 and B7-H1. M31A, N33A, H96A, and K98A display significantly reduced binding compared to the wild-type (around 42%–67% of wild type) (Figure 6; Supplemental Table S2), suggesting that they directly participate in, but are not absolutely required for, ligand binding. Consistent with their important roles in ligand binding, all of the altered residues in these mutants, except M31 and H96, are identical in human and murine PD-1 (Figure 5C). Sequence conservation of residues important for ligand binding between murine and human PD-1 indicates that murine B7-H1 recognizes similar binding surfaces on murine and human PD-1, in agreement with the observed similar binding of B7-H1 by these two receptors.

Q55S, V57A, and P97A have moderately decreased affinities for the ligand compared to the wild-type (around 83%–88% of wild type), whereas N51A and L53A bind the ligand as well as the wild-type of PD-1 (Figure 6; Supplemental Table S2). Interestingly, D29A, D29S, and A99L display approximately 10%–20% higher binding to the ligand than the wild-type (Figure 6; Supplemental Table S2). The observation that the A99L mutation increased rather than abolished ligand binding was surprising, as it was predicted that the substitution of Ala with a bulky Leu residue would cause steric hindrance in the binding interface, and consequently, prevent PD-1 from interacting with B7-H1. However, considering the high inherent flexibility of the CDR3 loop suggested by the crystal structure, the bulky side chain

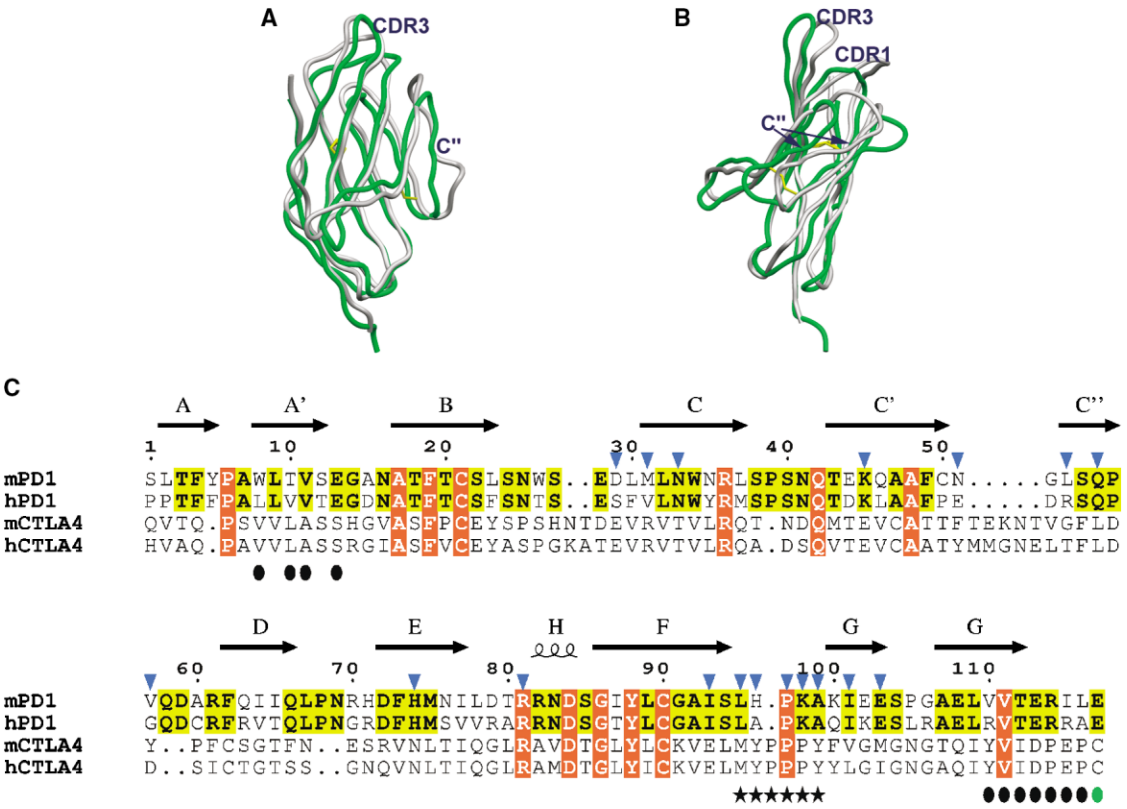

Figure 5. Comparison of Murine PD-1 and CTLA-4

(A and B) Two orthogonal views of a superimposition of murine PD-1 (green) and CTLA-4 (gray) structures. Parts with significant differences between the two structures are labeled.

(C) Structure-based sequence alignment of PD-1 and CTLA-4. Identical residues between murine and human PD-1 are colored in yellow, whereas invariant residues between PD-1 and CTLA-4 are colored in red. Residues in murine PD-1 selected for mutation are highlighted with closed squares in blue. Residues in CTLA-4 involved in homodimerization and B7 binding (the MYPPPY loop) are highlighted with closed circles and closed squares, respectively. Cys122 mediating the interchain disulfide in CTLA-4 is highlighted with closed circles in green; a Glu residue occupies the equivalent position in PD-1.

of Leu99 might be readily accommodated by a local conformational adjustment upon the engagement of the ligand. Notably, the double mutant D29A/A99L exhibits approximately 35% higher ligand binding than the wild-type, suggesting an additive effect caused by the D29A and A99L single mutations (Figure 6E; Supplemental Table S2). Taken together, these results demonstrate that the residues altered in these mutants do not contribute significant binding energy to the PD-1/B7-H1 interaction. H74S and R81S, located on the back sheet and the interface between the front and back sheets, respectively, both exhibit ligand binding activities similar to the wild-type (Figures 6E and 6F; Supplemental Table S2). These observations are consistent with the conclusion that the ligand binding surface resides solely on the front face of PD-1 (Figure 7A).

Discussion

The present study shows that PD-1 is monomeric both in solution and on the cell surface, in contrast to CTLA-4, CD28, and ICOS, which are all obligate disulfide-linked homodimers (Carreno and Collins, 2002; Schwartz et al., 2002). The structures of the CTLA-4/B7 complexes (Schwartz et al., 2001; Stamper et al., 2001) and the disulfide-linked dimer of unliganded CTLA-4 (J.-C.D.S. and X.Z., unpublished data) have shown that the dimerization interface of CTLA-4 is formed by nearly invariant residues located C-terminal to the G strand and residues centered around the A′ strand. (Figure 5C). The analogous regions in PD-1 are not highly conserved between human and murine sequences (~60% identity in these regions versus ~65% identity in the whole extracellular domain) (Figure 5C), suggesting that these regions do not play a central role in the structure and function of PD-1. It should be noted that even in the absence of the interchain disulfide, a significant proportion of CTLA-4 exists as a noncovalent dimer in solution, demonstrating its inherent tendency to self-associate (Zhang et al., 2002). These observations imply an intrinsic difference between PD-1 and CTLA-4, and by extension, perhaps CD28 and ICOS as well. Importantly, the dimeric nature of the CTLA-4 and B7 molecules are critical features of the alternating lattice of the CTLA-4/B7 complexes that have been proposed to play a role in CTLA-4-mediated signal transduction (Schwartz et al., 2001; Stamper et al., 2001). Therefore, the monomeric nature of PD-1 suggests that this molecule might signal through a distinct

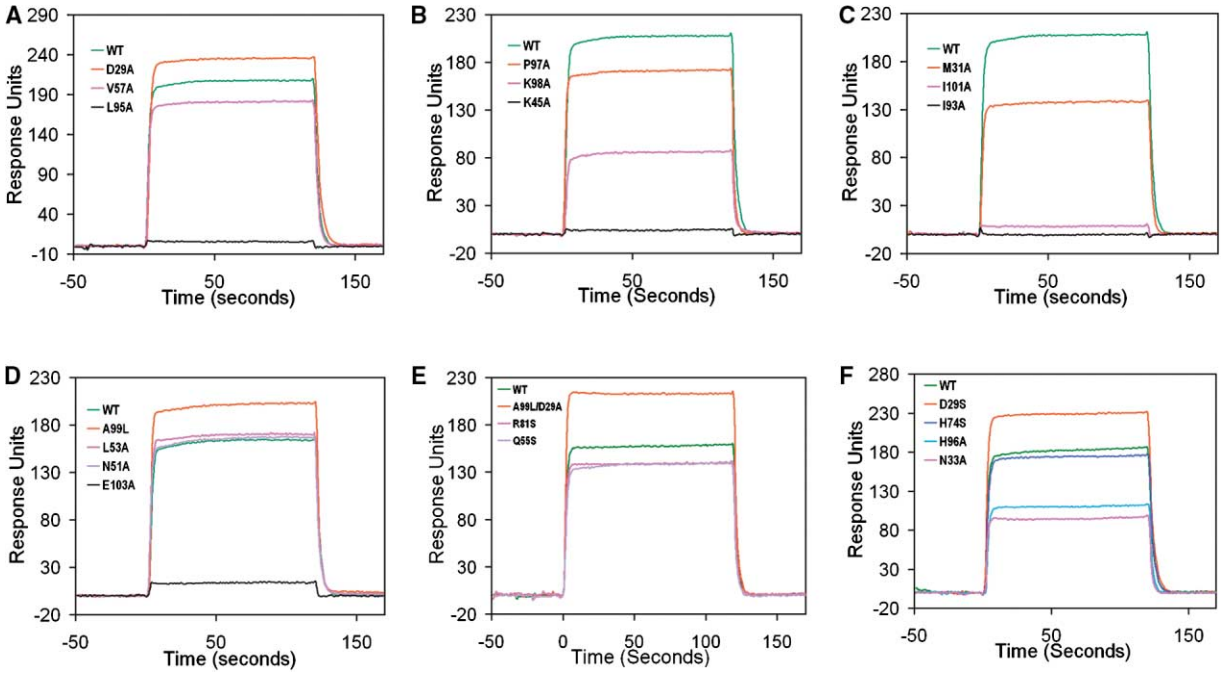

Figure 6. Ligand-Binding Activities of the Murine PD-1 Mutants

The wild-type and mutants of HA-tagged murine PD-1 at 1.7 μM were injected at 20 μl/min for 2 min over CM5 sensor chips coupled with murine B7-H1-Ig fusion protein. The final response of each protein was calculated by subtracting the response of the control cell from that of the experimental cell. The response levels of the mutants were compared with that of the wild-type protein to obtain the relative ligand-binding activities of the mutants.

mechanism, such as ligand-induced dimerization, oligomerization, or conformational alterations. However, at present, a more detailed model of the signaling complex cannot be proposed since there are no data regarding the in vitro or in vivo oligomerization state of the PD-1 ligands. While the present studies demonstrate that a significant fraction of the PD-1 molecules exist as monomers on the cell surface, the spectroscopic techniques utilized cannot rule out the presence of a small and transient population of clustered PD-1 molecules, as has been recently demonstrated for CD40 (Reyes-Moreno et al., 2003).

Receptor/ligand binding assays demonstrate that bacterially expressed murine PD-1 lacking carbohydrate binds to murine PD-L1-Ig fusion protein with a K_d of ~4 μM. These observations demonstrate that, as has been previously shown for human CTLA-4 and B7-2 (Schwartz et al., 2001; Stamper et al., 2001; Zhang et al., 2002), glycosylation is not required for the ligand binding activity of PD-1. There are four potential glycosylation sites in the Ig V-type domain of murine PD-1. Three of these four sites, N16 (in the A′B loop), N41 (in the CC′ loop) and N83 (in the EF loop), are located distal to the ligand binding surface on the front face and most likely do not directly affect ligand binding of PD-1 (Figure 1A). However, glycosylation of these sites in vivo could provide restraints on the orientation of PD-1 on the cell surface and indirectly affect PD-1/PD-L interaction in the immunological synapse, as has been previously suggested for CD2 and ICAM-2 (Davis et al., 1998; Wang and Springer, 1998). The fourth site, N25, located in the CDR1 loop (BC loop) is in close proximity to the F and G strands, which are identified by our mutagenesis studies as major contributors to the ligand binding surface. Glycosylation of this site might influence the local structure, and consequently, could have some impact on the affinity of PD-1 for ligand. The qualitative features of the binding and dissociation phases of the sensorgrams suggest that the k_{on} and k_{off} of the PD-1/B7-H1 interaction are rapid, similar to that observed for the CTLA-4/B7 complexes (Figure 3) (Collins et al., 2002).

The crystal structure of PD-1 provided critical information for rational mutagenesis studies, which resulted in an outline of the ligand binding surface on this costimulatory receptor. The hydrophobic residues identified to be critical for ligand binding (I93, L95, and I101) all cluster in the hydrophobic patch on the front face of murine PD-1. These residues are surrounded by the three charged residues (K45, K98, and E103) and two polar residues (N33 and H96) that are also involved in the PD-1/B7-H1 interaction (Figures 1 and 7). The hydrophobic center (I93, L95, and I101) and charged residues (K45 and E103) contribute significant binding energy to the receptor/ligand interaction, as indicated by the complete loss of ligand binding upon the mutation of these residues. Other polar residues surrounding the hydrophobic patch (N33, H96, K98) may mainly function in stabilizing the orientation between the receptor and ligand and determining the specificity of the interaction, as mutation of these residues results in reduced, but not abolished, ligand binding. The ligand binding surface in CTLA-4 is also composed of a cluster of hydrophobic residues (the MYPPPY CDR3 loop) and several hydrophilic residues (E33, R35, T53, and E97) (Figure 7B)

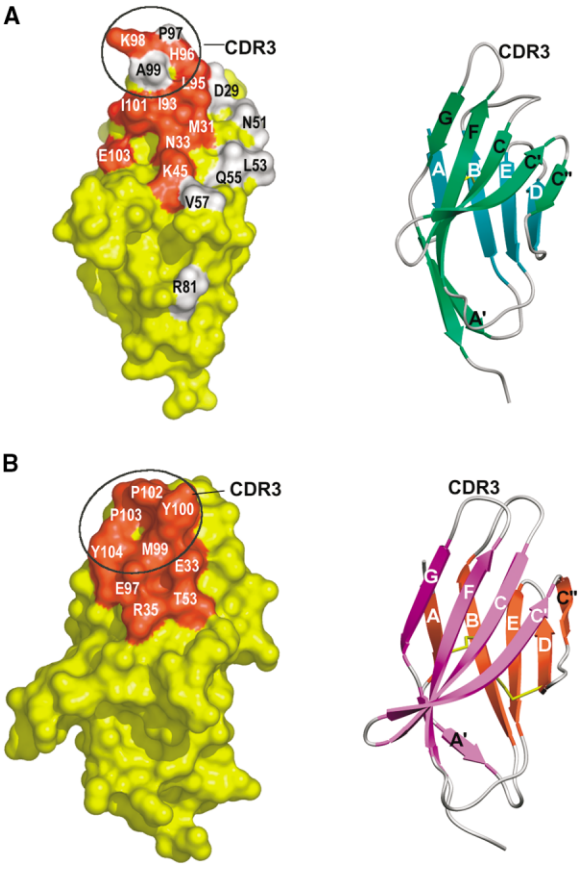

Figure 7. Comparison of Ligand-Binding Surfaces of PD-1 and CTLA-4

(A) Molecular surface of murine PD-1. Residues whose mutations resulted in abolished or significantly reduced ligand binding are colored in red, whereas residues whose mutations had no significant effects on ligand binding or led to higher ligand binding are colored in gray. The ribbon diagram is shown on the right to indicate the orientation of the molecule.

(B) Molecular surface of human CTLA-4 from the CTLA-4/B7-2 complex (Schwartz et al., 2001). Residues involved in ligand binding are colored in red. The ribbon diagram is shown on the right to indicate the orientation of the molecule. The CDR3 loops in both PD-1 (A) and CTLA-4 (B) are circled and labeled, showing the different contributions of this loop to ligand binding for these two receptors.

(Schwartz et al., 2001; Stamper et al., 2001). However, this surface of CTLA-4 is organized differently, in that the hydrophilic residues are located close to one another, forming a patch that is adjacent to the hydrophobic area. A more notable difference between the ligand binding surfaces of PD-1 and CTLA-4 is the role of the CDR3 loop in ligand binding. Structural studies reveal that the CDR3 loop of CTLA-4 is a major contributor to the binding interface and mutagenesis studies demonstrate that these residues are indispensable for ligand binding (Metzler et al., 1997; Morton et al., 1996; Schwartz et al., 2001; Stamper et al., 2001). The CDR3 loop of CTLA-4 adopts an unusual cis-trans-*cis* conformation and is very rigid, as shown by all the available crystal structures of CTLA-4. In contrast, the CDR3 loop of PD-1 exhibits considerable flexibility with weak electron density and relatively high B factors. Furthermore, mutagenesis studies show that residues in the CDR3 loop of murine PD-1 are not critical determinants for the PD-1/B7-H1 interaction. None of the four residues selected for mutagenesis (H96, P97, K98, and A99) in the CDR3 loop are absolutely required for ligand binding of PD-1 (Figure 7A; Supplemental Table S2). Consistent with their modest roles in ligand binding, residues in the CDR3 loop are not strictly conserved between murine and human PD-1 (Figure 5C). In contrast, the residues identified to be critical for ligand binding (K45, I93, L95, I101, and E103) are all contributed from strands in the front face.

Interestingly, a recent mutagenesis study on the ligands of murine PD-1 has also shown that residues from the strands on the front faces, but not those in the CDR3 loops, of both murine B7-H1 and B7-DC are required for binding PD-1(Wang et al., 2003). Taken together, these mutagenesis data on both the receptor and ligands suggest that the complexes of PD-1 and its ligands adopt an orthogonal binding mode similar to that of the CD2/CD58 complex (Wang et al., 1999) such that strands from the front faces of the receptor and ligands make the major contribution to the receptor/ligand interface, whereas the CDR3 loops reside at the periphery of the interface and do not make critical atomic contacts. This interpretation suggests a strand-to-strand binding mode for the PD-1/PD-L complexes, which is distinct from the loop-to-strand binding mode observed in the CTLA-4/B7 complexes and also thought to be relevant to the CD28/B7 and ICOS/ B7RP-1 costimulatory complexes (Schwartz et al., 2001; Stamper et al., 2001).

The mutagenesis study has also identified a few PD-1 mutants (D29A, D29S, A99L, and D29A/A99L) with slightly improved binding to the ligand compared to the wild-type. The observation of these moderately higher affinity mutants suggests the possibility of designing additional PD-1 mutants with even higher ligand binding affinities. Given the recent implication of PD-1 signaling in tumor immune evasion (Dong et al., 2002; Iwai et al., 2002), such reagents may prove valuable for the development of immuno-therapy against various malignancies.

In summary, PD-1 has been shown to be monomeric both in solution and when expressed on the cell surface. In addition, structure-based mutagenesis studies have identified the unique surface of PD-1 responsible for binding ligand. These findings suggest significant structural and functional differences between PD-1 and other members of the costimulatory receptor family.

Experimental Procedures

Cloning, Expression, and Purification of the Extracellular Ig V-Type Domains of Murine and Human PD-1

The extracellular region of murine PD-1 with the unpaired Cys50 mutated to Ser was amplified by two-step PCR using the full-length murine PD-1 cDNA as the template as described for ICOS by Wang et al. (2002). The flanking 5′ primer (incorporating an NdeI site and the start codon) and 3′ primers (incorporating a BamHI site) were 5′GAGGCTCATATGTCCCTCACCTTCTACCCAGCC3′ and 5′ACGG GATCCTCACTCCAGGATTCTCTCTGTTAC3′, respectively. The two middle complementary primers containing the Cys to Ser mutation were 5′ACTGAAAAACAGGCCGCCTTCTCTAATGGTTTGAGCCAAC CCGTC3′ and 5′GACGGGTTGGCTCAAACCATTAGAGAAGGCGGC CTGTTTTTCAGT3′. The PCR product was sequenced and cloned

into pET3a vector predigested with NdeI and BamHI as described for B7-2 previously (Zhang et al., 2002). Using this pET3a vector containing the PD-1 insert as the template, a HA-tagged derivative of wild-type murine PD-1 was amplified by PCR. The same flanking 5′ primer was used. The flanking 3′ primer (including the sequences that encode 3 linker residues and the HA tag) was 5′GTAGGATCCT CAAGCGTAGTCTGGAACATCATACGGGTAGGAGCCACCTGAGGT CTCCAGGATTCTCTC3′. The same mutagenesis strategy was employed to amplify the HA-tagged mutants of PD-1 (D29A, D29S, M31A, N33A K45A, N51A, L53A, Q55A, Q55S, V57A, H74S, R81S, I93A, L95A, H96A, P97A, K98A, A99L, I101A, and E103A) for ligand binding assays using middle complementary primers containing desired mutations. A D29A/A99L double mutant was generated using the D29A pET3a plasmid as the template. The extracellular Ig V-type domain of human PD-1 (129 amino acid residues excluding the initiator Met) was also cloned with the unpaired Cys60 mutated to Ser. The flanking 5′ primer and 3′ primers were 5′GAGGCTCATATG TGGAACCCCCCCACCTTCTCC3′ and 5′GTAGGATCCTCAGGGT GAGGGGCTGGGGTGGGC3′, respectively. The two middle complementary primers containing the Cys to Ser mutation were 5′CGCAG CCAGCCCGGCCAGGACTCCCGCTTCCGTGTCACACAACTG3′ and 5′CAGTTGTGTGACACGGAAGCGGGAGTCCTGGCCGGGCTGGCT GCG3′. The HA-tagged versions of the wild-type and mutants were prepared as they represent a highly useful reagent set for future experiments.

The proteins were expressed and refolded as described for B7-2 (Zhang et al., 2002). The wild-type murine PD-1 was purified by gel filtration (Superdex G75, 30X1.0) followed by anion exchange (MonoQ, 1 ml) chromatography to produce protein of >99% purity for crystallization. The HA-tagged wild-type and mutants of murine PD-1 were purified to >95% homogeneity by gel filtration chromatography for SPR receptor/ligand binding assays. Human PD-1 was similarly purified by gel filtration chromatography.

FRET Analyses for Murine PD-1 on the Cell Surface

Full-length murine PD-1 was amplified by PCR using a 5′-primer: 5′ATCAGATCTGCCACCATGTGGGTCCGGCAGGTACCC3′ and 3′-primer: 5′GGCGACCGGTGGAAGAGGCCAAGAACAATGTCC3′. A short version of murine PD-1 with the cytoplasmic tail trimmed to 10 residues was amplified using a 3′-primer: 5′GGCGACCGGTG GAGTGTCGTCCTTGCTTCCAGC3′. The PCR products were double digested with BglII and AgeI and cloned into predigested pECFP and pEYFP vectors. The sequences of the genes were confirmed by DNA sequencing. Full-length murine CTLA-4 was also cloned into the same set of vectors and used as positive controls. Tandem CFP-YFP protein, another positive control, was made by fusing murine B7-1 to 5′ end of CFP, which in turn was cloned into pEYFP vector. In this tandem CFP-YFP construct, the CFP and YFP are expressed on a single polypeptide chain separated by seven amino acid residues. The CFP and YFP constructs were cotransfected using Fugene 6 (Roche Biochemicals) into CHO cells grown on cover slips. 24–36 hr posttransfection, cells were fixed with 2% paraformaldehyde and examined with a Leica TCS SP 2 AOBS laser-scanning confocal microscope. CFP was excited with 405 nm light and emission monitored over the range of 416–492 nm; YFP was excited with 514 nm light and emission monitored over the range of 525–600 nm. YFP was photobleached using the 514 nm laser line at full power for 1–2 min. An image of CFP fluorescence and YFP fluorescence after photobleaching was obtained using the respective filter sets. Data were collected from 10–12 different cells in different fields from the same coverslip. Two to three regions of interest (located on the cell membrane) in the photobleached area were selected per cell and the mean CFP fluorescence before and after photobleaching was obtained using the Leica Confocal software. FRET efficiency was calculated using the following relationship: $FRET_{eff} = (D_{post}-D_{pre})/D_{post}$ where D_{post} is the fluorescence intensity of the CFP (donor; D) after photobleaching and D_{pre} is the fluorescence intensity of the CFP before photobleaching. A FRET efficiency of 5% was considered as the threshold for establishing a significant signal. Students t test (two tailed) was performed to demonstrate the level of significance between various groups.

Analytical Ultracentrifugation Analyses for Murine PD-1

Purified murine PD-1 was exchanged into a buffer containing 10 mM Tris-HCl and 100 mM NaCl (pH 8.0) using an Amicon concentrator with a 5 kDa cut-off membrane before the experiments. Sedimentation equilibrium analysis was performed at protein concentrations of 11.3, 22.6, and 37.6 μM (0.15, 0.3, and 0.5 mg/ml) in a Beckman analytical ultracentrifuge using an AN-60 Ti rotor at 4°C. The partial specific volume of murine PD-1 was calculated to be 0.721 $cm^3\ g^{-1}$ based on the amino acid composition. Buffer density was determined to be 1.0040 $cm^3\ g^{-1}$ using a Mettler De40 density meter operated at the experimental temperature. Absorbance scans were taken after 24 and 26 hr and equilibrium was assumed to have been reached if the results were unchanged. Data were collected at rotor speeds of 25,000 rpm and 34,000 rpm after equilibrium was reached and analyzed using Beckman XL-A/XL-I software v4. Analyses consisted of six scans taken of the three different nominal concentrations at each of the two rotor speeds.

SPR Binding Assays for PD-1 and B7-H1-Ig Fusion Protein

All binding experiments were carried out using a BIAcore X optical biosensor at 25°C. Research grade CM5 sensor chips were activated by a 7 min injection of a 1:1 mixture of NHS and EDC from the amine coupling kit at a flow rate of 5 μl/min. 7–15 μl of mB7-H1-Ig fusion protein (50 μg/ml) in 10 mM acetate buffer (pH 5.0) were injected over the experimental flow cell and immobilized to the sensor surface by free amine coupling chemistry, which typically resulted in immobilization levels of 3500–4000 RUs. 35 μl of 1 M ethanolamine (pH 8.5) was then injected for 7 min to deactivate both the experimental and reference flow cells. A sensor chip coupled with a misfolded murine B7-DC protein produced in the lab was used as a negative control for the binding assays. For determining the binding affinity of the wild-type murine PD-1 for mB7-H1-Ig, 16 serial dilutions of the PD-1 protein, starting from 78.0 μM and 1.4-fold dilution thereof, were prepared in HBS-EP buffer composed of 10 mM HEPES (pH 7.4), 150 mM NaCl, 3 mM EDTA, and 0.005% surfactant P20. Protein samples of different concentrations were sequentially injected over both flow cells at a flow rate of 20 μl/min for 2 min. Background responses of the reference flow cell were subtracted from the total responses of the experimental flow cell to give the final response levels. Each experiment was repeated three times and the average was taken as the final result. Purified human B7-2 Ig V-type domain at various concentrations in HBS-EP buffer was injected as negative control, which resulted in response levels of ~0 RU. Murine PD-1 was injected to the negative control sensor chip, which also generated response levels of ~0 RU. These results confirm that the detected binding is the specific interaction between PD-1 and the ligand. Equilibrium dissociation constants were obtained by fitting the data using nonlinear 1:1 Langmuir binding model and linear 1:1 binding Scatchard plot. The following equations were used for the nonlinear and linear fits:

$$R = R_{max}C/(C + K_d) \text{ (non-linear 1:1 Langmuir binding model)}$$

$$R/C = -C/K_d + R_{max}/K_d \text{ (linear 1:1 Scatchard plot)}$$

Where R is the bound analyte in RUs, R_{max} is the maximum response level, C is the concentration of free analyte in μM, and K_d is the equilibrium dissociation constant in μM.

The HA-tagged mutants of murine PD-1 were injected and the response levels were compared with that of the HA-tagged wild-type protein injected at the same concentration to obtain the relative ligand binding abilities of the mutants. A protein concentration of 1.7 μM (0.025 mg/ml) was used in these assays because this concentration of wild-type protein yielded high enough, but far from saturating, levels of SPR response shown by the experiments for affinity measurement. All of the experiments were repeated at least two times and the differences between the repeats were negligible (<1%). The cross-species interaction of human PD-1 with murine B7-H1-Ig fusion protein was measured using the same protocol.

Crystallization, Data Collection, and Structure Determination

Murine PD-1 was crystallized by the hanging drop vapor diffusion method by mixing 2 μl of protein at 6 mg/ml and 2 μl of crystallization buffer composed of 20%–30% PEG 8000, 100 mM NaAc, and 100 mM NaCacodylate (pH 6.5). Crystals were flash cooled to 100 K under a stream of nitrogen gas in the crystallization buffer supplemented with 15% Glycerol before data collection. Diffraction data

from a single crystal were collected to 2.0 Å resolution at beamline X9B (National Synchrotron Light Source, Brookhaven National Laboratory) using a 2X2 ADSC CCD Detector. The data were consistent with the orthorhombic space group $P2_12_12_1$ (a = 23.97, b = 50.80, c = 75.28 Å). Data were processed with the HKL suite (Otwinowski and Minor, 1997) and data collection statistics are summarized in Supplemental Table S1.

A BLAST search of the NCBI database suggested that the Ig V-type domain of a TCRα chain (Vα-2.6) was the most homologous molecule to PD-1 (25% identity). The crystal structure of this Ig V-type domain (PDB Number 1B88), with all of the nonidentical residues between the model and PD-1 mutated to Ala or kept unchanged if the original residue is a Gly, was used as the search model for molecular replacement trials performed with the program EPMR at 4.0 Å resolution (Kissinger et al., 1999). The best solution with a single monomer of the model molecule from molecular replacement has a correlation coefficient of 0.25 as calculated by EPMR. Rigid body refinement of this model at 2.2 Å resolution using the program CNS (Brunger et al., 1998) resulted in an R_{factor} of 54.4%. Despite the high R_{factor}, a $2F_o$-F_c electron density map calculated at 2.2 Å resolution was readily interpretable, with continuous densities for most of the β strands. Modeling and refinement at 2.0 Å resolution (including torsion angle dynamic simulated annealing, bulk solvent correction, and individual B factor refinement) were performed by using the program O (Jones et al., 1991) and CNS, respectively. The final model contains all the residues of murine PD-1, except the C-terminal residue Glu and the side-chains of His96, Pro97, and Lys100, and 73 H_20 molecules, with R_{cryst} and R_{free} of 19.82% and 22.83%, respectively. Structure refinement statistics are summarized in Supplemental Table S1.

Molecular superimpositions and rms deviation calculations were performed with FIT (G. Lu, http://bioinfo1.mbfys.lu.se/guoguang/fit.html). Structure-based sequence alignment was rendered with the program ESPript (Gouet et al., 1999). Molecular surfaces were generated with grasp (Nicholls et al., 1991) or Pymol (DeLano W.L., http://www.pymol.org). Ribbon diagrams were generated with Setor (Evans, 1993).

Acknowledgments

We thank Dr. T. DiLorenzo and M. Roden for insightful discussions, Dr. Z. Dauter for assistance with data collection, and Dr. M. Brenowitz and S. Morris for assistance with analytical ultracentrifugation experiments. This work is supported by grants from the National Institutes of Health to L.C., M.A.E., S.G.N., and S.C.A. X.G. and Z.-Y.Z. are supported in part by the G. Harold and Leila Y. Mathers Charitable Foundation.

References

Agata, Y., Kawasaki, A., Nishimura, H., Ishida, Y., Tsubata, T., Yagita, H., and Honjo, T. (1996). Expression of the PD-1 antigen on the surface of stimulated mouse T and B lymphocytes. Int. Immunol. *8*, 765–772.

Bogan, A.A., and Thorn, K.S. (1998). Anatomy of hot spots in protein interfaces. J. Mol. Biol. *280*, 1–9.

Brunger, A.T., Adams, P.D., Clore, G.M., DeLano, W.L., Gros, P., Grosse-Kunstleve, R.W., Jiang, J.S., Kuszewski, J., Nilges, M., Pannu, N.S., et al. (1998). Crystallography and NMR system: a new software suite for macromolecular structure determination. Acta Crystallogr. D Biol. Crystallogr. *54*, 905–921.

Carreno, B.M., and Collins, M. (2002). The B7 family of ligands and its receptors: new pathways for costimulation and inhibition of immune responses. Annu. Rev. Immunol. *20*, 29–53.

Collins, A.V., Brodie, D.W., Gilbert, R.J., Iaboni, A., Manso-Sancho, R., Walse, B., Stuart, D.I., van der Merwe, P.A., and Davis, S.J. (2002). The interaction properties of costimulatory molecules revisited. Immunity *17*, 201–210.

Davis, S.J., Ikemizu, S., Wild, M.K., and van der Merwe, P.A. (1998). CD2 and the nature of protein interactions mediating cell-cell recognition. Immunol. Rev. *163*, 217–236.

Dong, H., Zhu, G., Tamada, K., and Chen, L. (1999). B7–H1, a third member of the B7 family, co-stimulates T-cell proliferation and interleukin-10 secretion. Nat. Med. *5*, 1365–1369.

Dong, H., Strome, S.E., Salomao, D.R., Tamura, H., Hirano, F., Flies, D.B., Roche, P.C., Lu, J., Zhu, G., Tamada, K., et al. (2002). Tumor-associated B7–H1 promotes T-cell apoptosis: a potential mechanism of immune evasion. Nat. Med. *8*, 793–800.

Evans, S.V. (1993). SETOR: hardware-lighted three-dimensional solid model representations of macromolecules. J Mol Graph *11*, 134–138.

Finger, L.R., Pu, J., Wasserman, R., Vibhakar, R., Louie, E., Hardy, R.R., Burrows, P.D., and Billips, L.G. (1997). The human PD-1 gene: complete cDNA, genomic organization, and developmentally regulated expression in B cell progenitors. Gene *197*, 177–187.

Freeman, G.J., Long, A.J., Iwai, Y., Bourque, K., Chernova, T., Nishimura, H., Fitz, L.J., Malenkovich, N., Okazaki, T., Byrne, M.C., et al. (2000). Engagement of the PD-1 immunoinhibitory receptor by a novel B7 family member leads to negative regulation of lymphocyte activation. J. Exp. Med. *192*, 1027–1034.

Gouet, P., Courcelle, E., Stuart, D.I., and Metoz, F. (1999). ESPript: analysis of multiple sequence alignments in PostScript. Bioinformatics *15*, 305–308.

Iwai, Y., Ishida, M., Tanaka, Y., Okazaki, T., Honjo, T., and Minato, N. (2002). Involvement of PD-L1 on tumor cells in the escape from host immune system and tumor immunotherapy by PD-L1 blockade. Proc. Natl. Acad. Sci. USA *99*, 12293–12297.

Jones, T.A., Zou, J.Y., Cowan, S.W., and Kjeldgaard, M. (1991). Improved methods for binding protein models in electron density maps and the location of errors in these models. Acta Crystallogr. A *47*, 110–119.

Kenworthy, A.K., and Edidin, M. (1998). Distribution of a glycosylphosphatidylinositol-anchored protein at the apical surface of MDCK cells examined at a resolution of <100 A using imaging fluorescence resonance energy transfer. J. Cell Biol. *142*, 69–84.

Kissinger, C.R., Gehlhaar, D.K., and Fogel, D.B. (1999). Rapid automated molecular replacement by evolutionary search. Acta Crystallogr. D Biol. Crystallogr. *55*, 484–491.

Latchman, Y., Wood, C.R., Chernova, T., Chaudhary, D., Borde, M., Chernova, I., Iwai, Y., Long, A.J., Brown, J.A., Nunes, R., et al. (2001). PD-L2 is a second ligand for PD-1 and inhibits T cell activation. Nat. Immunol. *2*, 261–268.

Metzler, W.J., Bajorath, J., Fenderson, W., Shaw, S.Y., Constantine, K.L., Naemura, J., Leytze, G., Peach, R.J., Lavoie, T.B., Mueller, L., et al. (1997). Solution structure of human CTLA-4 and delineation of a CD80/CD86 binding site conserved in CD28. Nat. Struct. Biol. *4*, 527–531.

Morton, P.A., Fu, X.T., Stewart, J.A., Giacoletto, K.S., White, S.L., Leysath, C.E., Evans, R.J., Shieh, J.J., and Karr, R.W. (1996). Differential effects of CTLA-4 substitutions on the binding of human CD80 (B7–1) and CD86 (B7–2). J. Immunol. *156*, 1047–1054.

Nicholls, A., Sharp, K.A., and Honig, B. (1991). Protein folding and association: insights from the interfacial and thermodynamic properties of hydrocarbons. Proteins *11*, 281–296.

Nishimura, H., Nose, M., Hiai, H., Minato, N., and Honjo, T. (1999). Development of lupus-like autoimmune diseases by disruption of the PD-1 gene encoding an ITIM motif-carrying immunoreceptor. Immunity *11*, 141–151.

Nishimura, H., Okazaki, T., Tanaka, Y., Nakatani, K., Hara, M., Matsumori, A., Sasayama, S., Mizoguchi, A., Hiai, H., Minato, N., et al. (2001). Autoimmune dilated cardiomyopathy in PD-1 receptor-deficient mice. Science *291*, 319–322.

Okazaki, T., Maeda, A., Nishimura, H., Kurosaki, T., and Honjo, T. (2001). PD-1 immunoreceptor inhibits B cell receptor-mediated signaling by recruiting src homology 2-domain-containing tyrosine phosphatase 2 to phosphotyrosine. Proc. Natl. Acad. Sci. USA *98*, 13866–13871.

Ostrov, D.A., Shi, W., Schwartz, J.C., Almo, S.C., and Nathenson, S.G. (2000). Structure of murine CTLA-4 and its role in modulating T cell responsiveness. Science *290*, 816–819.

Otwinowski, Z., and Minor, W. (1997). Processing of X-ray diffraction data collected in oscillation mode. Methods Enzymol. *276*, 307–326.

Pentcheva, T., and Edidin, M. (2001). Clustering of peptide-loaded MHC class I molecules for endoplasmic reticulum export imaged by fluorescence resonance energy transfer. J. Immunol. *166*, 6625–6632.

Reyes-Moreno, C., Girouard, J., Lapointe, R., Darveau, A., and Mourad, W. (2003). CD40/CD40 homodimers are required for CD40-induced phosphatidylinositol-3 kinase-dependent expression of B7.2 by human B cells. J. Biol. Chem. *279*, 7799–7806.

Schwartz, J.C., Zhang, X., Nathenson, S.G., and Almo, S.C. (2002). Structural mechanisms of costimulation. Nat. Immunol. *3*, 427–434.

Schwartz, J.C., Zhang, X., Fedorov, A.A., Nathenson, S.G., and Almo, S.C. (2001). Structural basis for co-stimulation by the human CTLA-4/B7–2 complex. Nature *410*, 604–608.

Sharpe, A.H., and Freeman, G.J. (2002). The B7–CD28 superfamily. Nat. Rev. Immunol. *2*, 116–126.

Stamper, C.C., Zhang, Y., Tobin, J.F., Erbe, D.V., Ikemizu, S., Davis, S.J., Stahl, M.L., Seehra, J., Somers, W.S., and Mosyak, L. (2001). Crystal structure of the B7-1/CTLA-4 complex that inhibits human immune responses. Nature *410*, 608–611.

Tseng, S.Y., Otsuji, M., Gorski, K., Huang, X., Slansky, J.E., Pai, S.I., Shalabi, A., Shin, T., Pardoll, D.M., and Tsuchiya, H. (2001). B7-DC, a new dendritic cell molecule with potent costimulatory properties for T cells. J. Exp. Med. *193*, 839–846.

Wang, J., and Springer, T.A. (1998). Structural specializations of immunoglobulin superfamily members for adhesion to integrins and viruses. Immunol. Rev. *163*, 197–215.

Wang, J.H., Smolyar, A., Tan, K., Liu, J.H., Kim, M., Sun, Z.Y., Wagner, G., and Reinherz, E.L. (1999). Structure of a heterophilic adhesion complex between the human CD2 and CD58 (LFA-3) counterreceptors. Cell *97*, 791–803.

Wang, S., Zhu, G., Tamada, K., Chen, L., and Bajorath, J. (2002). Ligand binding sites of inducible costimulator and high avidity mutants with improved function. J. Exp. Med. *195*, 1033–1041.

Wang, S., Bajorath, J., Flies, D.B., Dong, H., Honjo, T., and Chen, L. (2003). Molecular modeling and functional mapping of B7–H1 and B7-DC uncouple costimulatory function from PD-1 interaction. J. Exp. Med. *197*, 1083–1091.

Zhang, X., Schwartz, J.C., Almo, S.C., and Nathenson, S.G. (2002). Expression, refolding, purification, molecular characterization, crystallization, and preliminary X-ray analysis of the receptor binding domain of human B7–2. Protein Expr. Purif. *25*, 105–113.

Accession Numbers

Coordinates and structure factors have been deposited in the PDB under accession code 1NPU.